Published in final edited form as:
Regen Med. 2009 March ; 4(2): 205–223. doi:10.2217/17460751.4.2.205.

Connexin43 carboxyl-terminal peptides reduce scar progenitor and promote regenerative healing following skin wounding

Gautam S Ghatnekar[1,2], **Michael P O'Quinn**[3], **L Jane Jourdan**[3], **Abhijit A Gurjarpadhye**[3], **Robert L Draughn**[4], and **Robert G Gourdie**[3,5,6]

[1] Comparative Medicine, Medical University of South, Carolina, Charleston, SC, USA

[2] FirstString Research Inc., North Charleston, SC, USA

[3] Departments of Cell Biology, & Anatomy, Medical University, of South Carolina, 171 Ashley, Avenue, Charleston, SC 29425-22204, USA, Tel.: +1 843 792 8181; Fax: +1 843 792 0664; E-mail: gourdier@musc.edu

[4] Materials Science, Medical, University of South Carolina, Charleston, SC, USA

[5] Pediatric Cardiology, Medical, University of South Carolina, Charleston, SC, USA

[6] Clemson-Medical University, of South Carolina Joint, Bioengineering Program, Medical University of South, Carolina, Charleston, SC, USA

Abstract

Aim—Gap-junctional connexin43 (Cx43) has roles in multiple aspects of skin wound healing – including scarring. The aim here was to study the effects of a cell-permeant peptide from the Cx43 carboxyl-terminus (CT) on scarring and regeneration following cutaneous injury.

Materials & methods—The effects of Cx43 CT peptide were studied in mouse and pig models of cutaneous injury. The parameters assessed included neutrophil density, wound closure, granulation, regeneration and skin tensile properties.

Results—Cx43 CT-peptide prompted decreases in area of scar progenitor tissue and promoted restoration of dermal histoarchitecture and mechanical strength following wounding of skin. These changes in healing were preceded by peptide-induced reduction in inflammatory neutrophil infiltration and alterations in the organization of epidermal Cx43, including increased connexon aggregation.

Conclusion—Cx43 CT peptide promotes regenerative healing of cutaneous wounds and may have applications in tissues other than skin, including heart, cornea and spinal cord.

Keywords

Cx43; gap junctions; regenerative medicine; scar prevention; wound healing

Correspondence to: Robert G Gourdie.

Future perspective

Scarring and abrogated histocomplexity are normal sequalae of trauma, including that resulting from implanted materials such as tissue-engineered scaffolds [55]. In ongoing work we are testing whether Cx43 CT peptides have therapeutic applications in implant biocompatibility, as well as in promoting regenerative healing of injured heart, cornea, retina and spinal cord.

Ethical conduct of research

The authors state that they have obtained appropriate institutional review board approval or have followed the principles outlined in the Declaration of Helsinki for all human or animal experimental investigations. In addition, for investigations involving human subjects, informed consent has been obtained from the participants involved.

The gap junction (GJ) is an aggregate of intercellular channels that provides for direct cell-to-cell interchange of metabolites, ions and other small molecules of approximately 1000 Da or less [1,2]. The individual channels of GJ aggregates in vertebrates are composed of integral membrane proteins encoded by the connexin family of genes, of which more than 20 members have been recognized [3]. It is well established that GJs, and the connexin subunits of GJs, function in various aspects of wound healing [4–6]. Reports for such functions have included roles for GJs and connexins in intercellular spread of injury signal, immune cell extravasation, inflammation, re-epithelization, wound closure and formation of the scar progenitor, granulation tissue. Intercellular communication is thought to be one aspect of GJ-based mechanisms regulating and affecting the response of tissues to injury [4,6–10]. There is also mounting evidence that connexins may contribute to wound repair processes without recourse to direct cell–cell communication [5,11].

The connexins show differential patterns of expression within skin [12–18]. Mutations in connexins have been linked to inherited cutaneous disease in humans [19,20]. Connexin43 (Cx43) is expressed in the dermal and epidermal layers of skin [13,14,16–18,21]. Previous studies have demonstrated the effects of targeting Cx43 in skin wound healing [13,14,21,22]. In a study by Becker, Green and co-workers, downregulation of Cx43 mRNA by antisense in mouse was demonstrated to accelerate healing following skin wounding, associated with upregulated expression of TGF-β1 mRNA, promotion of fibroblast proliferation and motility *in vitro* and more active granulation *in vivo* [14,21]. In another report from the same group, it was shown that a similar antisense strategy enhanced re-epithelization of a diabetic skin model in mouse [22]. While the mechanism of Cx43 action remains to be determined, Cx43 has recently been identified as a direct and positive regulator of the TGF-β signaling, promoting the release of Smad2 bound to β-tubulin [23].

The C-terminus (CT) of Cx43 is a substantial (>120 amino acids) and important regulatory domain [2,10]. We reported on a 25 amino acid peptide comprised of an antennapedia cell internalization sequence linked to the CT-most nine amino acids of the full-length Cx43 CT domain [24]. This short sequence incorporates multiple protein binding sites including a postsynpatic density 95/discs large/zonula occludens-1 (PDZ) class II-binding motif. The peptide has been demonstrated to bind to the second PDZ domain (PDZ2) of zonula occludens (ZO)-1, thereby competitively inhibiting the interaction of endogenous Cx43 molecules with ZO-1. ZO-1 is a member of the membrane-associated guanylate kinase (MAGUK) family of proteins and was originally discovered via its association with the tight junction [25]. In addition to interacting with actin, connexins and tight junction proteins, ZO-1 has been shown to bind to components of cadherin-containing junctions [26] and may function in re-epthelialization of the cornea following injury [27].

In earlier studies of Cx43-expressing cells *in vitro* we showed that the inhibitory peptide reduced ZO-1 localization at the periphery of GJs and mediated increases in size of GJ channel aggregates, without affecting bulk levels of Cx43 [24]. The rationale for studies of the effect of the Cx43 CT peptide in skin wound healing *in vivo* came initially from observations made in ‘scratch wound’ assays of fibroblast monolayers *in vitro* [28]. Our data indicate that the inhibitory peptide reduces the area of granulation tissue and promotes regeneration of cutaneous structure/function following cutaneous injury *in vivo*. These changes to the healing progression are presaged by inhibition of neutrophil infiltration and acute alterations in Cx43 organization in wound epidermal cells, including increased GJ size in response to the inhibitory peptide.

Materials & methods

Animals

All procedures were performed in accordance with the Guide for Use of Experimental Animals at the Medical University of South Carolina (South Carolina, USA) and conformed to the NIH Animal Care and Use Guidelines (Publication No. 85–23, revised 1985).

Anesthesia—Adult 3–4 month old CD-1 mice (Charles River Laboratories, Wilmington, MA, USA) were anesthetized using a combination of ketamine at 75 mg/kg (Fort Dodge Laboratories Inc., Fort Dodge, IA, USA), xylazine at 15 mg/kg (LLOYD Laboratories, Shenandoah, IA, USA), and acepromazine at 0.2 mg/kg (Boehringer Ingelheim, St. Joseph, MO, USA). Neonatal mice were sedated by placing them on ice to induce hypothermia. Swine 20–25 kg (Palmetto Research Swine, Reevesville, SC, USA) were preanesthetized with ketamine 33 mg/kg and acepromazine 1.1 mg/kg subcutaneously followed by induction with 1.5 minimum alveolar concentration isofluorane.

Peptide sequences—α–connexin carboxyl-terminal (ACT1) peptide corresponds to a short sequence at the Cx43 CT linked to an antennapedia internalization sequence (RQPKIWFPNRRKPWKKRPRPDDLEI) as described and characterized by Hunter *et al.* [24]. A peptide comprising only the antennapedia portion of the ACT1 peptide sequence (RQPKIWFPNRRKPWKK) was used as a control. Other Cx43 peptides used include ACT2 (RPRPDDLEI), and ACT3C (RQPKIWFPNRRKPWKK RPSSRASSRASSRPRPDDLEI). All peptides were synthesized by American Peptide Co. Inc. (CA, USA) or Peptron Inc. (South Korea).

Detection of peptide *in vivo* & antibody protocols—Three-day old mouse pups were desensitized using hypothermia. A 4 mm incisional skin wound was made using a scalpel through the entire thickness of the skin (down to the level of the underlying muscle) in the dorsal midline between the shoulder blades. A 30 μl solution of 30% pluronic (F-127, stock No. P2443, Sigma, MO, USA) gel containing either no or dissolved peptide at a concentration of 60 μM was then applied to the incisional injuries. Skin samples were collected at 2 and 6 h postwounding to determine peptide levels in the samples using anti-Cx43 (stock no. C6219, Sigma, MO, USA) immunoblots, streptavidin alkaline phosphatase (AP; stock no. S921, Molecular Probes, OR, USA) blotting and fluor-conjugated streptavidin microscopy as previously detailed in Hunter *et al.* [24].

Western blot analysis—Skin samples were flash frozen in liquid nitrogen and then stored at −70°C until processing. Frozen tissue was pulverized in a liquid nitrogen prechilled biopulverizer to a fine powder. The powdered samples were then added to a tube containing 900 μl of lysis buffer (50mMTris-HCL, pH7.5, 1% Triton-X-100, 1% sodium deoxycholate, 0.5% SDS, 0.01 M ethylenediaminetetra-acetic acid, 0.05 M NaF, 1 mM dithiothreitol, 1 mM phenylmethanesulphonylfluoride, 1 mM Na3VO4, Roche complete mini's). Lysates were rotated at 4°C for 30 min with vortexing at 10 min intervals. Samples were triturated using a syringe with a 22-guage needle six times and incubated with vortexing at regular intervals for an additional 60 min. The samples were then cleared by centrifugation at 10,000 rpm for 10 min. Protein concentration was determined by Bio-Rad Micro-BCA (Fisher Scientific, VA, USA). 75 μg samples were heated at 95°C in Lammeli sample buffer for 5 min. Samples were resolved on a 10–20% Tris-HCL Criterion 345–0042 gel, and transferred at 12 V for 20 min on Bio-Rad semi-dry apparatus to PVDF Immobilon-PSQ, 0.2 μm membrane (Fisher Scientific, VA, USA). The membrane was rinsed, and blocked in 5% bovine serum albumin/ Tris-buffered saline Tween-20 for 1 h. For detection using antibodies against Cx43 CT, primary antibody (Sigma C6219 1:2000 in block) was added and incubated overnight at 4°C. Secondary

antibodies at 1:10000 (goat antirabbit AP SBI 4010–4014, Biotin-AP Molecular Probes S-921) were added and incubated at room temperature for 1.5 h. AP was detected with Tropix CDP-Star chemiluminesence followed by Nitro-Blue tetrazolium chloride/5-bromo-4-chloro-3′-indolyphosphate p-toluidine colorimetric development. For detection of the biotin tag on the amino terminal in blots, streptavidin horse radish peroxidase (HRP; GE Healthcare, Piscataway, NJ, USA) was used as described in Hunter *et al.* [24].

***In situ* detection of peptide—**A number of 2 mm punch excisions were made on 3-day old neonatal mice. To detect the distribution of peptide, whole-mount skin samples from the wounded area were dissected 2 h post-application of 60 μM ACT1 peptide, fixed in 2% paraformaldehyde at 40°C for 20 min and washed in PBS. Subsequently, samples were incubated in streptavidin (Alexa 594) (Molecular Probes, Eugene, OR, USA), at 1:500 for 3 h at room temperature. Following staining, samples were washed three times for 1 h each, mounted and imaged as a whole mount on a Leica SP2 laser scanning confocal microscope (LSCM).

Immunohistochemistry—Double immunolabeling was undertaken using antibodies against Cx43 and ZO-1, as described previously [24]. Measurements of immunolabeled Cx43 GJ particle size, numerical density and overall area of Cx43 was as described previously [24, 28]. Microscopy was undertaken using a Leica SP2 LSCM using standard modalities.

Skin wound models

Full-thickness 4mm incisional wounds on neonatal CD-1 mice were treated with either 20% pluronic (F-127, stock no. P2443, Sigma, USA) gel vehicle containing either no (i.e., control, n = 12) or dissolved 60 μM ACT1 peptide (i.e., treatment, n = 12). Peptide in this, and subsequent experiments, was applied to wounds twice, first immediately after wounding and a second time 24 h later. Wounds were imaged using a Leica MZ FLIII stereomicroscope with an attached Hamamatzu C5180 RGB camera linked to a computer at 6 and 24 h, and 2, 3, 4 and 7 days postwounding. Full-thickness 5 mm excisional wounds on adult CD-1 mice were treated with 20% pluronic gel containing either no (i.e., control, n = 102) or dissolved 60 μM ACT1 peptide (i.e., treatment, n = 95). Mice were anesthetized as described above and wounds were imaged at 1, 4, 7 and 10 days postwounding, except for two experiments that were extended beyond 10 days for imaging at 15, 21, and 30 days postwounding. Data were accumulated in nine independent experiments with 8–16 animals each in treatment and control groups in each experiment. Over 700 wound images were measured for closure, as well as redness, and scarring (see later). For pigs, six full-thickness 1 cm excisional wounds, three each at paired locations on either side of the dorsal midline. Wounds on one side received ACT1 and the opposite side of the animal received a vehicle control. A 500 μl solution of 20% pluronic gel containing either no or dissolved peptide at a concentration of 100 μM was then applied to the injuries. The wounds were monitored for 30 days and then biopsied under anesthesia.

Histological & functional assessments of healing Wound redness & scarring on adult mouse wounds

The images of adult mouse excisional wounds from the nine experiments were visually scored by two independent observers blind to treatment for redness/swelling at 24-h and 4-day time-points, and overall appearance/scarring (i.e., relative degree of discoloration and smoothness) 7 and 10 days postwounding, using methods similar to those described by Qiu *et al.* [14]. Each wound was assigned a score from 0–5 by each observer and the final score for each wound was the mean score of the two observers. For the redness index, a lower number corresponded to a reduced presumed level of initial inflammation. For overall appearance/scarring, a higher number was assigned to wounds with a higher relative degree of discoloration and increased

smoothness. For quantitative assessment of wound closure, area of each wound at each time point was measured blind to treatment using ImageJ software.

Neutrophil density in neonatal wounds—Neutrophil density was assessed using a novel whole-mount technique. Two day-old neonatal mouse pups were desensitized by hypothermia. Full-thickness excisional wounds of 2 mm were made at least 1cm apart on either side of the dorsal midline using a 2 mm disposable biopsy punch (Miltex, Inc. Tuttlingen, Germany). Wounds were treated with either 60 μM ACT1 peptide or no peptide (vehicle control) in the wound beds – one treatment and one control per mouse. Whole-mount skin samples (pelts) containing both peptide and control wound pairs were obtained at 6 h (n = 6), 24 h (n = 7) and 48 h (n = 11) postwounding – treatment was repeated at 24 h postwounding for the 48 h time point. Pelts were rinsed in PBS, pinned to sylguard dishes, and reacted in Hanker-Yates Reagent (Sigma −3901–10VL): 10 mg/ml, 0.1 M Tris-HCl pH 7.6, 0.03% H_2O_2, 1% Triton-X-100 at 4°C for 15 min. The whole mounts were rinsed in PBS, flattened with glass shards and fixed overnight in 4% paraformaldehyde. The flattened and fixed samples were rinsed in water, dehydrated through 50, 75 and 100% alcohol series, and cleared to transparency using benzyl alcohol and benzyl benzoate 1:2 (Sigma, MO, USA). The cleared whole mounts were mounted ventrodorsal in benzyl benzoate and montage imaged using a 5× objective on a Leica leica microscope trademark (DMLR) microscope. Following generation of montages of each wound, a digital grid was placed over the montage and the total number of myeloperoxidase-reacted cells was counted square by square blind to treatment to give an estimate of all neutrophils recruited to that wound. Neutrophils were counted on 21 montages of the whole mounts, each comprises 30–50 images taken using a 5× objective on a Leica DMLR microscope and digital camera.

Neutrophil density in adult wounds—Owing to the increased thickness of skin with age, a similar whole-mount approach to that used in neonates could not be used to assess neutrophil recruitment in adults. The thickness of adult skin affects the ability to stain, fix and clear whole mounts. More importantly, owing to the numerical aperture of the objective, imaging of the total neutrophil density throughout the axial width of adult skin samples was not possible. Skin samples from adult mouse excisional skin injuries were obtained at 24 h and 4 days postwounding, paraffin embedded and sectioned at 10 μm. Three treatment and three control wounds were assessed at the two time points. Five cross sections in the dorsoventral plane through the center of each wound were stained with H&E using standard protocols. Neutrophils were counted in four standardized locations per section within the wound site based on the characteristic nuclear morphology of these cells using a 63× objective on a Leica DMLR microscope.

Epidermal neogenesis, granulation area & vascular density measurements—Paraffin-embedded tissue sections were obtained for histological analysis using standard procedures. Counts of epidermal rete pegs [29] were carried out in 20× fields using H&E-stained 10 μm tissue sections. For mice, four control and four treatment excisional wounds were measured. For pigs, three treatment and three control wounds were measured. Granulation area was measured in the same wounds (five and three sections from the wound center for mice and swine respectively) using images from 5× objective fields taken with the Leica DMLR microscope and digital camera.

Quantification of α-smooth muscle actin-positive (sma^+) cells were undertaken on sections through unwounded pig skin and from the center of the same excisional wounds used for rete peg counts. Immunofluorescent-labeling for sma was undertaken as described in Hewett *et al.* [30]. DAPI-positive nuclei colocalized with sma^+ in vascular structures were counted in 40× fields taken using the Leica DMLR microscope in fluorescence mode with attached digital camera. Eight images were taken per section and three sections were sampled from each of the

three treatment and three control wounds (i.e., n = 6 with 24 images sampled from each wound for the quantification).

Tensile strength measurements—As we have described previously, breaking stress/tenacity and extension of a biological material stretched until failure will correlate with the mechanical properties of its weakest element [31]. For a strip of tissue of uniform material properties, this weakest element will generally correspond to its segment of narrowest cross-sectional dimension with respect to the axis of strain. For a strip of uniform dimensions, but of variable composition, the element that fails will correlate with the tissue sector composed of the weakest material in the strip. We thus tested narrow (5 mm at their narrowest width) strips of skin of constant dimensions **(**Figure 8B) to failure, to obtain mechanical stress and strain at break indices for the weakest structural element within these skin strips. Prior to testing, the thickness of strips was measured at the segment of narrowest width by Vernier caliper for the purpose of calculating breaking stress. No significant difference in thickness was detected between treatment and control groups. Testing was done on a MTS 858 Mini Bionix tensile strength testing machine (MTS Systems Corporation, MN, USA) equipped with a 5 kg load cell. The strips of skin containing healed mouse wounds at 30 (n = 4 control, n = 6 treatment) and 90 days (n = 12 control, n = 12 treatment) postwounding were extended to failure. Gauge length was set at a constant 1 cm and the strip was extended-to-break at 0.5 mm/s. Tensile strength at break (stress), and extension-to-break (strain) were calculated from recorded force–extension charts as follows:

$$\begin{aligned} &\text{Stress}\,(N/mm^2) = \text{Force at break}\,(N)/ \\ &\text{cross sectional area of sample}\,(mm^2) \\ &\text{Strain}\,(\%) = [\,\text{Increase in length at break}\,(mm)/ \\ &\text{original length}\,(mm)\,] \times 100 \end{aligned}$$

The parameters for each wound skin strip were normalized to measurements obtained from an unwounded skin strip collected nearby from the same animal.

Statistical analysis

T-test was used for statistical analysis of data. Bonferroni's correction was applied. The Wilcoxin matched-pairs signed-ranks test was used for neutrophil counts in the whole-mount neutrophil assay.

Results

Effect on incisional wound healing in neonatal mice

The Cx43 CT peptide ACT1 **(**Figure 1A) was applied in 20% pluronic gel to full-thickness incisional wounds between the shoulder blades on the dorsal midline of 12 neonatal mice **(**Figure 1B–M). Over a 7-day time course, it was observed that peptide-treated wounds closed faster, appeared less swollen and inflamed, gaped less, and healed with a smoother, less-scarred appearance than control wounds (20% pluronic vehicle, n = 12). Of note, control wounds typically displayed swellings at the wound edge over the first 4 days postinjury **(**Figure 1I & J), that were not detectable or reduced in wounds at corresponding time points treated with peptide. We concluded that ACT1 treatment resulted in an altered progression of healing following incisional wounding in neonatal mice.

Distribution of ACT1 in wounded cutaneous tissue

Next, levels of peptide acutely present in and around wounded skin were assessed in neonatal mice. Figure 2 shows a western blot of ACT1 2 and 6 h postapplication as detected by an

antibody against the CT of Cx43 **(**Figure 2A) and binding of streptavidin-HRP to the biotinylated N-terminal of ACT1 **(**Figure 2B). The figure shows that ACT1 is detectable in wounds by the two probes at both time points, though is fainter at 6 h. Streptavidin detected the peptide as a single band less than 10 kDa. In the case of the antibody against the Cx43, the ACT1 band is observed, as well as prominent bands at 42–45 kDa consistent with phosphoisoforms of endogenous Cx43. Less prominent and faster-migrating polypeptides not corresponding to added exogenous peptide or full-length Cx43 were also present on blots of both wounded and nonwounded neonatal skin **(**Figure 2A).

To assess the spread of the Cx43 CT peptide following application to wounded tissue, we undertook confocal optical sectioning of whole-mount skin samples from neonates labeled with fluor-conjugated streptavidin to detect the biotinylated peptide 2 h postwounding. The peptide could be observed in tissues surrounding the wound edges **(**Figure 2C & E). However, fluorescent signal was not present in tissues surrounding control wounds that had received vehicle, but no peptide **(**Figure 2D & F).

Effect on excisional wound healing in adult mouse

After observing that ACT1 peptide altered wound healing in neonates, we next assessed excisional wounds in adult mice, using a similar strategy. As in neonates, excisional wounds in adult mice treated with peptide closed faster, appeared less swollen and inflamed, and healed with a less discolored appearance than control counterparts over a 10-day time course **(**Figure 3A–J). Quantification of wound closure demonstrated ($p < 0.0001$), and this difference was maintained at 4 ($p < 0.0001$), 7 ($p < 0.0001$) and 10 ($p < 0.01$) days postwounding **(**Figure 3K). These studies were undertaken in nine experiments each with eight to 16 animals in treatment and control groups. The p values for the effect of ACT1 in each of the nine experiments were 0.04, 0.02, 0.007, 0.005, 0.004, 0.024, 0.12, 0.05, 0.04 respectively; for instance, closure rate was significantly accelerated by ACT1 in eight of the nine experiments.

Qualitative assessments of redness and scarring/appearance of wounds were made by independent observers blind to treatment. Wounds treated with the Cx43 CT peptide demonstrated significantly reduced redness **(**Figure 3L) at 24 h ($p < 0.0001$) and 4 days ($p < 0.001$) postwounding and significantly improved overall appearance **(**Figure 3M) at 7 ($p < 0.0001$) and 10 ($p < 0.0001$) days postwounding. The improvement in the appearance of wounds was maintained ($p < 0.05$) in two further experiments that were extended beyond 10 days to 15, 21 and 30 days postwounding (data not shown).

Effect of molecules related to ACT1

In addition to ACT1 **(**Figure 3), we designed and/or tested a number of peptide variants on adult wounds **(**Figure 4A–E). These included a control peptide containing the antennapedia sequence incorporated within ACT1 peptide (Antp), a peptide corresponding to the CT nine amino acids of Cx43 with no attached antennapedia sequence (ACT2 peptide), a peptide comprising the antennapedia sequence linked to a nonconnexin class II PDZ-binding domain (from ErbB2) and a peptide comprising antennapedia sequences fused to the CT-most 21 amino acids of Cx43 (ACT3).

The effects of Antp alone **(**Figure 4B) was indistinguishable from that of pluronic vehicle **(**Figure 3F–J) and also from what could be seen on untreated wounds that had not been exposed to either peptide or vehicle **(**Figure 4A), suggesting that neither Antp nor pluronic gel accounted for the effects on wound closure of ACT1 treatment. Similarly, the peptide incorporating the ErbB2 CT sequence had no significant influence on closure, suggesting that the results for ACT1 were not a general property of PDZ-binding domains **(**Figure 4E). ACT3, the peptide containing the longer Cx43 CT sequence, accelerated wound closure compared with controls,

though to a lesser degree than ACT1 **(**Figure 4D). This suggested that while the longer ACT3 sequence promoted closure, the sequence necessary for optimized effects on healing was present in the last nine or fewer amino acids of the Cx43 CT. Interestingly, ACT2, the Cx43 CT sequence that did not incorporate N-terminal Antp, also accelerated closure **(**Figure 4C). Short peptides can be taken at reasonable efficiency by some cells. Arginines at the N-terminal of ACT2 may also confer cell-penetrating activity in the absence of antennapedia. However, ACT2 also did not increase closure rate to the same degree as ACT1, suggesting that intracellular delivery of the Cx43 CT was required for the efficient deployment of peptide bioactivity.

Effect on neutrophil density

Figures 1 & 3 suggested that ACT1 had affects on the early inflammatory response. We thus undertook quantitative analyses of effects on recruitment of neutrophils in neonatal and adult wounds **(**Figure 5). To do this a novel assay was developed. In brief, bilateral 2 mm excisions were made adjacent to the dorsal midline of neonatal mice, one wound being treated with ACT1, the other receiving vehicle control **(**Figure 5A–C). Rectangular 'pelts' containing ACT1-treated and control wounds on the same animal were obtained at 6 **(**Figure 5A), 24 **(**Figure 5B) and 48 h **(**Figure 5C) postwounding, myeloperoxidase-reacted to localize neutrophils, fixed and cleared to transparency with benzyl alcohol and benzyl benzoate. Using this technique, the distribution and number of all neutrophils within the full 3D volume of each wound field could be assessed.

There was a significant reduction ($p < 0.03–0.001$) in neutrophil density at ACT1-treated wounds relative to controls in neonates at all time points **(**Figure 5E). Consistent with the well-established pattern, neutrophil density peaked at 24 h, falling off at 48 h **(**Figure 5E). Neutrophils in ACT1-treated wounds were frequently sequestered in blood vessels **(**Figure 5C&D), suggesting that reduced recruitment of neutrophils in treated wounds may have resulted from inhibition of leukocyte transmigration.

Owing to the increased thickness of skin with age, a whole-mount approach could not be used to assess neutrophils in adults. Neutrophil numbers were therefore counted in histological sections taken within the midplane of ACT1-treated and control excisional wounds at 24 h and 4 days. Consistent with our results in neonates, significant decreases in the density of neutrophils were detected in ACT1-treated adult wounds relative to controls at both time points ($p < 0.01–0.001$) **(**Figure5F).

Effect on epidermis & granulation tissue

Epidermal structure and granulation tissue deposition were assessed in tissue sections from adult mouse excisional wounds at 10 days postwounding **(**Figure 6A–F). The newly formed epidermal layer covering control wounds was typically uniform, nonundulating and unlike unwounded skin **(**Figure 6D). The neoepidermal tissue in control wounds demonstrated little evidence of complexity, including an absence of epidermal invaginations known as rete pegs. By contrast, the epidermis of ACT1-treated wounds was histologically more complex **(**Figure 6A&B), displaying undulation, involution and a significant fourfold increase ($p < 0.05$) in rete pegs compared with controls **(**Figure 6E). In a complementary change in wound structure, measurements from histological sections indicated that granulation tissue area was significantly reduced ($p < 0.0001$) in ACT1-treated wounds relative to controls **(**Figure 6F).

The effects of ACT1 peptide on wound healing in adult mice led us to determine whether a similar response occurred in the pig. The swine is a well-accepted wound healing model owing to its relatively hairless, taut skin, said to resemble that of humans. As in mouse, peptide-treated pig wounds at 30 days postwounding demonstrated large numbers of rete pegs **(**Figure 6G &

H). By contrast, the healed epidermis of control wounds was distinctive in lacking rete pegs (Figure 6I & J). The difference in rete pegs between treatment and control was significant ($p < 0.0001$) (Figure 6K). ACT1-treated wounds also demonstrated a significant reduction ($p < 0.0002$) in granulation tissue area as compared with control wounds (Figure 6G–J&L).

Effect on dermal vascular pattern

Histological sections of the pig samples were stained using antibodies against sma to evaluate blood vessel density within unwounded skin and wound granulation tissue (Figure 7). Figure 7A–C are montages from sma-immunolabeled sections and show extended views that span from the epidermis to the dermal base. The section planes are identical to those illustrated in Figure 6G & I and the long axis of each montage is centered on the wound midline. In unwounded skin, sma^+ vessels were notably denser subepidermally than in the superficial dermis (Figure 7A). In sections of healed, ACT1-treated wounds, the density of sma^+ profiles in the subepidermis was also higher than in deeper regions of dermis, albeit not as elevated as in unwounded skin (compare Figure 7A & B). In contrast to unwounded and healed peptide-treated wounds, vehicle control wounds showed no evidence of increased subepidermal vascular density, instead displaying a uniform distribution of small blood vessels in granulation tissue from the superficial to the basal dermis. Counts of nuclei colocalized with sma^+ vascular profiles confirmed ($p < 0.05$) the qualitative assessment of an increased density of superficial blood vessels in unwounded skin and ACT1-treated wounds (Figure 7D–F). ACT1 treatment thus prompted a partial re-establishment of vascularization in the superficial dermis following wounding.

Effect on mechanical properties of healed skin

Thin strips of skin from healed excisional wounds and adjacent unwounded skin (from adult mice 1 and 3 months postinjury) were strained to break to assess the mechanical properties of wounded tissues at failure. Measurements at failure were carried out so that the tenacity and extensibility of the weakest material in the strip would be assessed; for instance, the healed wound or tissue at the interface of scar and normal cutaneous tissue. Figure 8A shows ACT1-treated and control wounds 3 months postwounding. As can be seen from these images, improvement in overall appearance of the healed wounds is maintained at 3 months. Representative force–extension curves are shown in Figure 8C & D. At 1 month, ACT1-treated wounds showed no significant improvement over controls for stress-at-break and strain-at-break. However, both indices of mechanical failure demonstrated significant increases at 3 months ($p < 0.05$) in peptide-treated wounds compared with controls (Figure 8E & F). The failure strain of ACT1-treated wounds at 3 months was 90% of unwounded skin (Figure 8F). By contrast, control wounds at 3 months remained only approximately 60% as extensible as normal skin at break (Figure8F).

Effects on epidermal Cx43 & ZO-1 protein distribution

Cx43 protein at the wound edge decreases naturally in the epidermis over 24–48 h [14,18]. Consistent with this, at 24 h we found that Cx43 immunolabeling levels were decreased in epidermal cells proximal to the wound compared with distal keratocytes in our standard mouse excisional injury model (Figure 9A–F). Moving from the wound edge, Cx43 particles (i.e., presumptive GJs) were first observed between basal epidermal cells, but were found at both basal and apical cells more distally (Figure 9E & F). ZO-1 immunolabeling was elevated in the cytoplasm of epidermal relative to dermal tissues. Apically located epidermal cells demonstrated prominent stripes of ZO-1 at cell borders (arrowheads, Figure 9E & F). There was a decrease in this apically localized staining in cells proximal to the wound edge and this reduction appeared to be more pronounced in ACT1-treated keratocytes than in controls. Cx43 was not co-localized within these apical stripes of ZO-1 immunolabeling. In general, elevated

levels of cytoplasmic ZO-1 in epidermal cells made assessment of Cx43-ZO-1 association problematic.

To investigate Cx43 levels and organization in the epidermis, well-established quantitative methods (e.g., [24]) were used to measure Cx43 particle size (i.e., Cx43 GJ size), particle numerical density and total area of immunolabeled Cx43 particles in paired peptide and control wounds on the same five adult mice **(**Figure 9G–I). To obtain information on how these Cx43 parameters varied in the epidermis as a function of proximity to the injury, measurements were undertaken from the wound edge in ten contiguous segments, each containing ten basal keratocytes in sequence (i.e., encompassing approximately 1 mm of epidermis from the wound edge). Total area of Cx43 immunolabeling in the epidermis did not significantly differ overall between ACT1 and control wounds. Similarly, the difference in total area of Cx43 between specific control and treated segments also did not reach p greater than 0.05. The numerical density of Cx43 particles was significantly ($p < 0.05$) reduced in peptide-treated wound epidermis relative to control between individual segments and overall – particularly in the segments of epidermis most distal from the wound edge **(**Figure 9G). The effect of treatment on number of Cx43 particles, but not total area of Cx43, was explained by a significant ($p < 0.05$) overall increase in the average size of Cx43 particles (i.e., GJs) occurring in ACT1-treated epidermal cells **(**Figure 9I).

Discussion

In this study, a membrane-permeant peptide incorporating the last nine amino acids of the Cx43 CT (ACT1) is shown to accelerate wound closure, enhance epidermal complexity, reduce granulation tissue area and increase breaking strength and extensibility of skin following cutaneous wounding in mice. The thick-skinned porcine model enabled resolution of a treatment-associated increase in superficial blood vessels that partially resembled the vascularization pattern of unwounded skin [32,33]. The changes in the healing progression of skin prompted by ACT1 were preceded by reductions in neutrophil recruitment, as well as changes in the subcellular organization of Cx43 in epidermal cells, including increases in the size of presumptive GJs.

The results here are consistent with extensive data indicating that inhibition of inflammation correlates with accelerated progression of cutaneous wound healing [10,34–42]. Following infiltration into the wound, hematopoietically derived cells (e.g., neutrophils and macrophages) generate reactive oxygen species, chemokines and cytokines that modulate chemotaxis and collagen deposition by scar-forming fibroblasts [10,41]. Prevention of such inputs by inflammatory cells may be a factor in the mode of action of ACT1 in reducing granulation tissue. However, it remains to be determined whether this is the primary explanatory factor of mechanism. One notable caveat comes from a study in which antineutrophil antibodies were used to induce transient neutropenia in mice [42]. While a loss of inflammatory infiltrate resulting from this treatment accelerated wound closure, no difference was found in collagen levels between control and neutropenic mice. Moreover, it appears that the precursors of neutrophils and macrophages are not the only circulating cells contributing to injury repair. Evidence is mounting that granulation tissue is in part derived from blood-borne progenitors called fibrocytes [43,44]. If circulating fibroblast progenitors were inhibited from infiltrating into the wound in a manner similar to that shown here for neutrophils (i.e., sequestration in blood vessels, inset Figure 5D), then a loss of cellular substrate may be another aspect of mechanism for ACT1-mediated reduction in the granulation tissue.

Scar vascularization in humans has not been reported to differ from that of unwounded skin [45]. Here, we demonstrate that newly differentiated granulation tissue in pig wounds displays a uniform distribution of blood vessels and loss of the vascularization normally found in the

dermal papillary layer. This difference may reflect species variance, although it is noteworthy that pigs and humans share related superficial to basal patterns of dermal vascularization [32, 33]. It may also arise because blood vessels take longer to repattern in the scar than the 30-day time course used in the present study. This being said, our data do indicate that the peptide prompted a partial re-establishment of superficial dermal vascularization in granulation tissue within a 30-day time period. Regenerative differentiation of dermis may contribute to the appearance of peptide-treated wounds, as also may the increased epidermal complexity apparently induced by ACT1 in pig and mouse. Epidermal rete pegs are present in unwounded skin and are thought to contribute to the appearance and mechanical properties of cutaneous tissues. Rete pegs also decrease with age – a change associated with reduced elasticity and increased fragility of skin in elderly people [46]. It has been long recognized by surgeons that 'give' (i.e., extensibility) in stitched wounds is beneficial to healing and scar reduction. The increases in rete pegs and improved mechanical characteristics **(**Figure 8E–F) of ACT1-treated wounds may thus have implications for healing of surgical lesions closed by primary intention.

Previous work has indicated that expression of an exogenous gene sequence encoding greater than 130 amino acids of the Cx43 CT inhibited proliferation associated with nuclear localization of the gene product [47]. This polypeptide comprised the entire 'cytoplasmic tail' of Cx43, including its many protein–protein interaction sites [10,48]. The antennapedia sequence incorporated in ACT1 targets its peptide cargo to the cytoplasm and not the nucleus [49]. Cytoplasmic targeting of ACT1 has been confirmed previously in HeLa cells [24]. Comparison between ACT1 and a longer 21-amino acid sequence **(**Figure 4D) furthermore indicates that optimized bioactivity in wound healing is specified with the CT-most nine amino acids of Cx43. In addition, the observed response to ACT1 also does not appear to be a universal property of PDZ-binding ligands, as treatment of wounds with a peptide incorporating the class II domain of ErbB2 **(**Figure 4E) did not elicit similar effects as ACT1. Lindsey *et al.* have demonstrated matrix metalloproteinase (MMP)7-mediated cleavage of the endogenous Cx43 CT in a cardiac wounding model [50]. *In silico* analysis of Cx43 identified consensus MMP sites generating peptides resembling ACT-like sequences including the CT-most 20 amino acids of Cx43. These data, together with the bioactivity of synthetic ACT peptides demonstrated in the present study, raise the intriguing prospect that short peptides proteolytically generated from the endogenous Cx43 CT may be part of a naturally occurring response to tissue injury.

In studies of Cx43-expressing HeLa cells, it has been shown that ACT1 prompts redistribution of Cx43 from a detergent-soluble to an insoluble fraction without causing changes in overall levels of the protein [24]. This repartitioning within the total pool of Cx43 is associated with an increase in levels of higher-mobility phosphorylated isoforms of the protein, and an increase in the size and decrease in the number of GJ aggregates [24]. Based on these data, we have proposed that ACT1-targeting of ZO-1–Cx43 interaction leads to a shift of connexon distribution from nonjunctional pools to sequestration within GJs. Studies of Cx43 mutants rendered incompetent for ZO-1 interaction further provide support for the concept that the protein–protein interaction targeted by ACT1 is involved in GJ size regulation [51,52]. The results shown here in epidermal cells parallel the observations reported *in vitro* [24]; namely, that ACT1 treatment is associated with increases in GJ size and reductions in GJ number, but does not alter overall levels of Cx43 protein.

Active downregulation of mRNA and protein has been proposed as a key aspect of the mechanism by which Cx43-targeting treatments, such as antisense, beneficially alter the healing progression of wound healing [14,21,22]. However, we would reiterate that our data continue to strongly indicate that ACT1 has no affect on protein levels in cells and tissues expressing Cx43 (e.g., Figure 9 and [24]. It is thus concluded that the mode of action of ACT1 is distinct from that of Cx43 antisense. The specifics of this novel mechanism remain to be

elucidated. The GJ size increase seen in epidermal cells proximal to the wound is further evidence that ACT1 prompts a shift in Cx43 distribution from nonjunctional to junctional pools. Whether or how an increase in the relative amounts of Cx43 sequestrated in GJ aggregates leads to accelerated wound healing remains to be understood. One avenue to further understand molecular mechanism may be to probe the unexpected linkage between Cx43 and TGFβ signaling identified initially by Hirschi, Dai and co-workers [53]. In particular it would be of interest to determine if and how shifts in the cellular distribution of Cx43 between nonjunctional and junctional pools affects the recently demonstrated ability of Cx43 to compete with Smad2 for β-tubulin binding [23]. As TGFβ activation is reduced by decreasing Cx43 in this model, reductions in nonjunctional Cx43 are an interesting aspect of ACT1 mechanism that warrant further exploration. That Cx43 not aggregated in GJs could be the locus of a regulatory interaction between the TGFβ pathway and Cx43 is consistent with a growing appreciation of nonjunctional roles for connexin proteins [5,11,54].

Conclusion

The Cx43 CT-peptide ACT1 promotes regenerative healing of cutaneous wounds. These changes in the healing progression are preceded by an ACT1-induced reduction in neutrophil infiltration and alterations in the organization of epidermal Cx43, including increased size of GJ aggregates.

Executive summary

- Prevention of scarring following cutaneous injury is an unmet clinical need. There is growing evidence of key roles for gap junctional connexin43 (Cx43) in wound healing – including in fibrotic scarring.
- Standardized mouse and pig models of skin wound healing were treated with α–connexin carboxyl-terminal (ACT1), a cell-permeant peptide incorporating a short sequence from the carboxyl-terminal (CT) of Cx43. Wounds were then assessed for structural and functional markers of inflammation, scarring and regenerative healing.
- The Cx43 CT peptide reduced the initial inflammatory response and area of scar progenitor tissue. Treatment was also associated with significant signs of regeneration including increased epidermal complexity and improvement of skin strength and extensibility.
- ACT1-mediated changes were not associated with downregulation of Cx43 in keratocytes, posited as a mechanistic aspect of how Cx43 targeting leads to enhanced wound healing. However, peptide bioactivity was marked by a change in the organization of Cx43 in the epidermis, as evidenced by increased gap junctional size.
- Additional therapeutic uses of ACT1 in implant biocompatibility and regenerative healing of injured heart, cornea, retina and spinal cord are currently being tested.

Acknowledgments

Financial & competing interests disclosure

This work was supported in part by grants from the NIH (R41AR053798, HL056728, and HL082802). RGG is also supported as a Medical University of South Carolina (MUSC) Board of Trustees Eminent Scholar. GS Ghatnekar is a founder, stockholder and CEO of FirstString Research Inc. (FSR). FSR is a biotechnology startup company spun-off from MUSC that is presently focused on funding and undertaking clinical trials on the safety and efficacy of ACT1 peptide in human skin wound healing applications. RG Gourdie is a founder, stockholder and member of the board of directors of FSR. The authors have no other relevant affiliations or financial involvement with any organization or

entity with a financial interest in or financial conflict with the subject matter or materials discussed in the manuscript apart from those disclosed.

No writing assistance was utilized in the production of this manuscript.

Bibliography

Papers of special note have been highlighted as:

▪ of interest

▪▪ of considerable interest

1▪. Bukauskas FF, Verselis VK. Gap junction channel gating. Biochim Biophys Acta 2004;1662(1–2): 42–60. [PubMed: 15033578]Along with [2], outstanding review series on connexin biology.

2▪▪. Jean-Claude H. The connexins. Biochim Biophys Acta 2004;1662(1–2):1–2. [PubMed: 15033575] Along with [1], outstanding review series on connexin biology.

3▪. Willecke K, Eiberger J, Degen J, et al. Structural and functional diversity of connexin genes in the mouse and human genome. Biol Chem 2002;383(5):725–737. [PubMed: 12108537]Excellent review.

4▪. Chanson M, Derouette JP, Roth I, et al. Gap junctional communication in tissue inflammation and repair. Biochim Biophys Acta 2005;1711(2):197–207. [PubMed: 15955304]Outstanding review series on connexin biology.

5. Bates DC, Sin WC, Aftab Q, Naus CC. Connexin43 enhances glioma invasion by a mechanism involving the carboxy terminus. Glia 2007;55(15):1554–1564. [PubMed: 17823969]

6. De Maio A, Vega VL, Contreras JE. Gap junctions, homeostasis, and injury. J Cell Physiol 2002;191 (3):269–282. [PubMed: 12012322]

7▪. King TJ, Lampe PD. Temporal regulation of connexin phosphorylation in embryonic and adult tissues. Biochim Biophys Acta 2005;1719(1–2):24–35. [PubMed: 16137642]Outstanding review series on connexin biology.

8. Lin JH, Weigel H, Cotrina ML, et al. Gap-junction-mediated propagation and amplification of cell injury. Nat Neurosci 1998;1(6):494–500. [PubMed: 10196547]

9▪. Ehrlich HP, Sun B, Saggers GC, Kromath F. Gap junction communications influence upon fibroblast synthesis of Type I collagen and fibronectin. J Cell Biochem 2006;98(4):735–743. [PubMed: 16475185]Useful study showing unexpected relationships between gap junctions (GJs) and matrix.

10▪. Rhett JM, Ghatnekar GS, Palatinus JA, et al. Novel therapies for scar reduction and regenerative healing of skin wounds. Trends Biotechnol 2008;26(4):173–180. [PubMed: 18295916]Recent review from the Gourdie laboratory.

11▪. Lin JH, Yang J, Liu S, et al. Connexin mediates gap junction-independent resistance to cellular injury. J Neurosci 2003;23:2, 430–441.Key study suggesting nonjunctional role for connexins in injury response

12. Djalilian AR, McGaughey D, Patel S, et al. Connexin 26 regulates epidermal barrier and wound remodeling and promotes psoriasiform response. J Clin Invest 2006;116(5):1243–1253. [PubMed: 16628254]

13. Kretz M, Maass K, Willecke K. Expression and function of connexins in the epidermis, analyzed with transgenic mouse mutants. Eur J Cell Biol 2004;83(11–12):647–654. [PubMed: 15679109]

14▪▪. Qiu C, Coutinho P, Frank S, et al. Targeting connexin43 expression accelerates the rate of wound repair. Curr Biol 2003;13(19):1697–1703. [PubMed: 14521835]Key study on connexin43 (Cx43) and skin wound healing

15. Saitoh M, Oyamada M, Oyamada Y, Kaku T, Mori M. Changes in the expression of gap junction proteins (connexins) in hamster tongue epithelium during wound healing and carcinogenesis. Carcinogenesis 1997;18(7):1319–1328. [PubMed: 9230274]

16. Coutinho P, Qiu C, Frank S, Tamber K, Becker D. Dynamic changes in connexin expression correlate with key events in the wound healing process. Cell Biol Int 2003;27(7):525–541. [PubMed: 12842092]

17▪. Richards TS, Dunn CA, Carter WG, Usui ML, Olerud JE, Lampe PD. Protein kinase C spatially and temporally regulates gap junctional communication during human wound repair via phosphorylation of connexin43 on serine368. J Cell Biol 2004;167(3):555–562. [PubMed: 15534005]Interesting study of role Cx43 CT phosphorylation and wound healing

18▪. Risek B, Klier FG, Gilula NB. Multiple gap junction genes are utilized during rat skin and hair development. Development 1992;116(3):639–651. [PubMed: 1289057]One of the first papers to identify Cx43 expression in cutaneous tissues

19. Richard G, Smith LE, Bailey RA, et al. Mutations in the human connexin gene *GJB3* cause erythrokeratodermia variabilis. Nat Genet 1998;20(4):366–369. [PubMed: 9843209]

20. Di WL, Common JE, Kelsell DP. Connexin 26 expression and mutation analysis in epidermal disease. Cell Commun Adhes 2001;8(4–6):415–418. [PubMed: 12064628]

21. Mori R, Power KT, Wang CM, Martin P, Becker DL. Acute downregulation of connexin43 at wound sites leads to a reduced inflammatory response, enhanced keratinocyte proliferation and wound fibroblast migration. J Cell Sci 2006;119(Pt 24):5193–5203. [PubMed: 17158921]

22. Wang CM, Lincoln J, Cook JE, Becker DL. Abnormal connexin expression underlies delayed wound healing in diabetic skin. Diabetes 2007;56(11):2809–2817. [PubMed: 17717278]

23▪▪. Dai P, Nakagami T, Tanaka H, Hitomi T, Takamatsu T. Cx43 mediates TGF-β signaling through competitive Smads binding to microtubules. Mol Biol Cell 2007;18(6):2264–2273. [PubMed: 17429065]Study directly implicating Cx43 CT in regulation of TGF-β signaling

24▪. Hunter AW, Barker RJ, Zhu C, Gourdie RG. Zonula occludens-1 alters connexin43 gap junction size and organization by influencing channel accretion. Mol Biol Cell 2005;16(12):5686–5698. [PubMed: 16195341]First description of ACT1 in a peer-reviewed journal

25▪▪. Mitic LL, Anderson JM. Molecular architecture of tight junctions. Annu Rev Physiol 1988;60:121–142. [PubMed: 9558457]Excellent review

26. Itoh M, Nagafuchi A, Moroi S, Tsukita S. Involvement of ZO-1 in cadherin-based cell adhesion through its direct binding to α catenin and actin filaments. J Cell Biol 1997;138(1):181–192. [PubMed: 9214391]

27▪. Taliana L, Benezra M, Greenberg RS, Masur SK, Bernstein AM. ZO-1: lamellipodial localization in a corneal fibroblast wound model. Invest Ophthalmol Vis Sci 2005;46(1):96–103. [PubMed: 15623760]Intriguing study implicating role for zonula occludens (ZO)-1 in corneal wound healing

28. Gourdie RG, Ghatnekar GS, O'quinn M, et al. The unstoppable connexin43 carboxyl-terminus: new roles in gap junction organization and wound healing. Ann NY Acad Sci 2006;1080:49–62. [PubMed: 17132774]

29. Kyriakides TR, Tam JW, Bornstein P. Accelerated wound healing in mice with a disruption of the thrombospondin 2 gene. J Invest Dermatol 1999;113(5):782–787. [PubMed: 10571734]

30. Hewett KW, Norman LW, Sedmera D, et al. Knockout of the neural and heart expressed gene HF-1β results in apical deficits of ventricular structure and activation. Cardiovasc Res 2005;67(3):548–560. [PubMed: 15907824]

31. Gourdie RG, Orwin DFG, Ranford S, Ross DA. Wool fibre tenacity and its relationship to staple strength. Aust J Agric Res 1992;43(8):1759–1776.

32. Churchill-Livingstone. Gray's Anatomy: The Anatomical Basis of Medicine and Surgery. 2004

33. Xie Y, Zhu KQ, Deubner H, et al. The microvasculature in cutaneous wound healing in the female red Duroc pig is similar to that in human hypertrophic scars and different from that in the female Yorkshire pig. J Burn Care Res 2007;28(3):500–506. [PubMed: 17438498]

34. Ashcroft GS, Yang X, Glick AB, et al. Mice lacking Smad3 show accelerated wound healing and an impaired local inflammatory response. Nat Cell Biol 1999;1(5):260–266. [PubMed: 10559937]

35. Bandyopadhyay B, Fan J, Guan S, et al. A "traffic control" role for TGFβ3: orchestrating dermal and epidermal cell motility during wound healing. J Cell Biol 2006;172(7):1093–1105. [PubMed: 16549496]

36. Coutinho P, Qiu C, Frank S, et al. Limiting burn extension by transient inhibition of Connexin43 expression at the site of injury. Br J Plast Surg 2005;58(5):658–667. [PubMed: 15927148]

37▪▪. Ferguson MW, O'Kane S. Scar-free healing: from embryonic mechanisms to adult therapeutic intervention. Philos Trans R Soc Lond B Biol Sci 2004;359(1445):839–850. [PubMed: 15293811] Review covering landmark contributions of Ferguson group to skin wound healing field

38. Martin P, D'Souza D, Martin J, et al. Wound healing in the PU.1 null mouse – tissue repair is not dependent on inflammatory cells. Curr Biol 2003;13(13):1122–1128. [PubMed: 12842011]

39. Qiu C, Coutinho P, Frank S, et al. Targeting connexin43 expression accelerates the rate of wound repair. Curr Biol 2003;13(19):1697–1703. [PubMed: 14521835]

40. Rhett JM, Ghatnekar GS, Palatinus JA, et al. Novel therapies for scar reduction and regenerative healing of skin wounds. Trends Biotechnol 2008;26(4):173–180. [PubMed: 18295916]

41▪▪. Clark, R. Wound repair overview and general considerations. In: Clark, R., editor. The Molecular and Cellular Biology of Wound Repair. Plenum Press; 1996. p. 3-50.A cutaneous wound healing bible

42▪▪. Dovi JV, He LK, DiPietro LA. Accelerated wound closure in neutrophil-depleted mice. J Leukoc Biol 2003;73:4, 448–455.Clever study that examines a role of neutrophils in skin wound healing

43▪. Stramer BM, Mori R, Martin P. The inflammation-fibrosis link? A Jekyll and Hyde role for blood cells during wound repair. J Invest Dermatol 2007;127(5):1009–1017. [PubMed: 17435786] Excellent review

44. Wang J, Jiao H, Stewart TL, et al. Accelerated wound healing in leukocyte-specific, protein 1-deficient mouse is associated with increased infiltration of leukocytes and fibrocytes. J Leukoc Biol 2007;82 (6):1554–1563. [PubMed: 18040084]

45. Amadeu T, Braune A, Mandarim-de-Lacerda C, Porto LC, Desmouliere A, Costa A. Vascularization pattern in hypertrophic scars and keloids: a stereological analysis. Pathol Res Pract 2003;199(7):469–473. [PubMed: 14521263]

46. Gilchrest BA. A review of skin ageing and its medical therapy. Br J Dermatol 1996;135(6):867–875. [PubMed: 8977705]

47. Dang X, Doble BW, Kardami E. The carboxy-tail of connexin-43 localizes to the nucleus and inhibits cell growth. Mol Cell Biochem 2003;242(1–2):35–38. [PubMed: 12619863]

48▪. Giepmans BN. Role of connexin43-interacting proteins at gap junctions. Adv Cardiol 2006;42:41–56. [PubMed: 16646583]Helpful review

49▪. Prochiantz A. Homeodomain-derived peptides. In and out of the cells. Ann NY Acad Sci 1999;886:172–179. [PubMed: 10667213]Useful review

50▪. Lindsey ML, Escobar GP, Mukherjee R, et al. Matrix metalloproteinase-7 affects connexin-43 levels, electrical conduction, and survival after myocardial infarction. Circulation 2006;113(25):2919–2928. [PubMed: 16769909]Intriguing study indicating peptidase generation of ACT-like fragments from the Cx43 CT occurs in response to cardiac injury *in vivo*

51▪. Maass K, Shibayama J, Chase SE, Willecke K, Delmar M. C-terminal truncation of connexin43 changes number, size, and localization of cardiac gap junction plaques. Circ Res 2007;101(12): 1283–1291. [PubMed: 17932323]Good paper examining effect of loss of Cx43 CT, including the ZO-1-binding domain, on cardiac GJ organization *in vivo*.

52. Hunter AW, Jourdan J, Gourdie RG. Fusion of GFP to the carboxyl terminus of connexin43 increases gap junction size in HeLa cells. Cell Commun Adhes 2003;10(4–6):211–214. [PubMed: 14681018]

53▪▪. Hirschi KK, Burt JM, Hirschi KD, Dai C. Gap junction communication mediates transforming growth factor-β activation and endothelial-induced mural cell differentiation. Circ Res 2003;93(5): 429–437. [PubMed: 12919949]First study to point to linkage between TGF-β and Cx43

54▪. Boengler K, Dodoni G, Rodriguez-Sinovas A, et al. Connexin43 in cardiomyocyte mitochondria and its increase by ischemic preconditioning. Cardiovasc Res 2005;67(2):234–244. [PubMed: 15919068]Interesting study showing an unexpected Cx43-mitochondrial association

55. Fauza DO, Fishman SJ, Mehegan K, Atala A. Videofetoscopically assisted fetal tissue engineering: skin replacement. J Pediatr Surg 1998;33(2):357–361. [PubMed: 9498417]

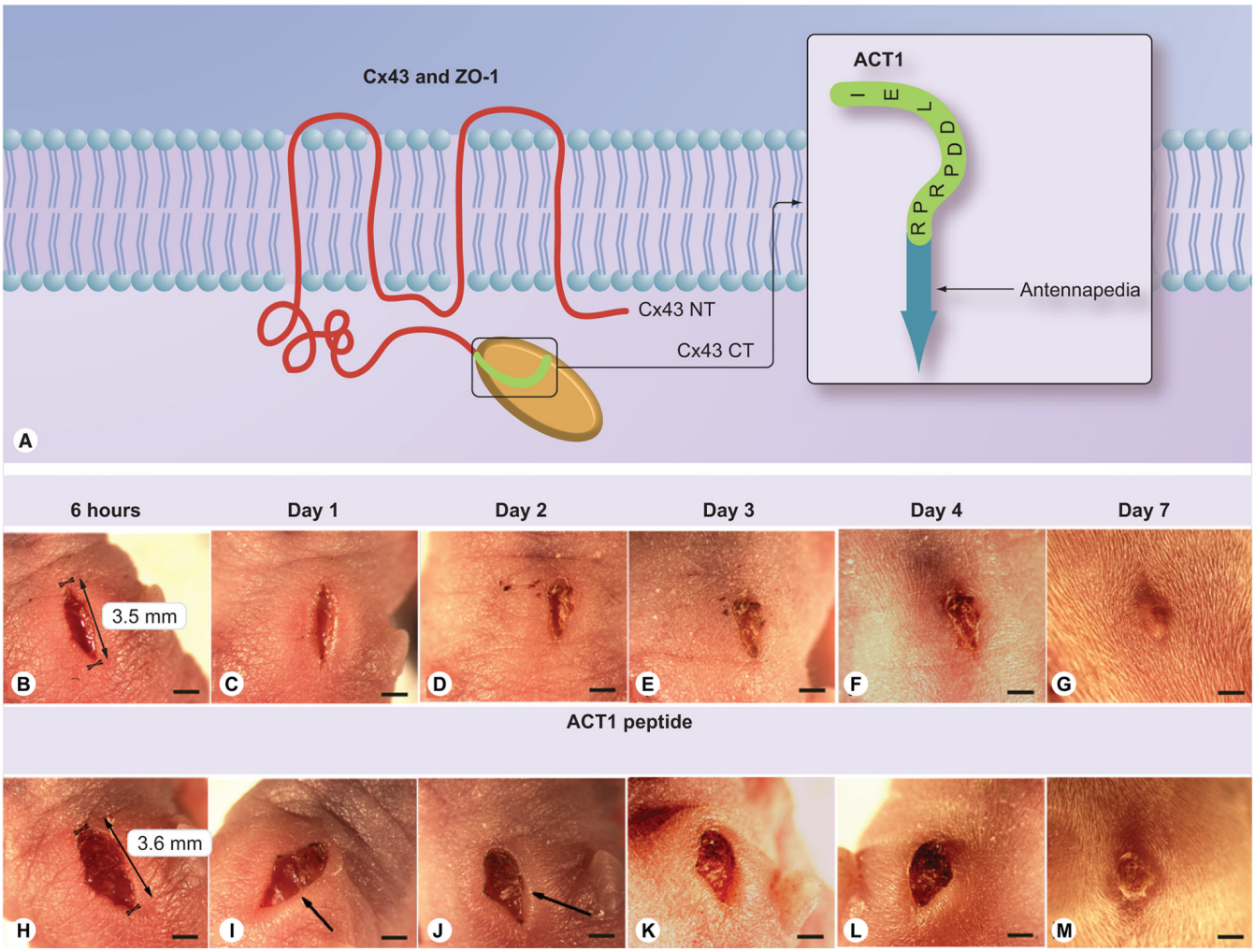

Figure 1. ACT1 and affects on healing of skin wounds on neonatal mice

(A) Model of Cx43 (red) in the lipid bilayer (blue) with its CT (green) bound to ZO-1 (orange). To the right, a model of ACT1. **(B–M)** The effect of ACT1 peptide on healing of an incisional wound on a neonatal mouse. Healing over 7 days following wounding and treatment with ACT1 **(B–G)** or vehicle control gel **(H–N)**. The treatment and control wounds shown are representative of 12 ACT1 and 12 control wounds. Arrows in figure I and J indicate swelling around the control wound, which is absent or reduced in the ACT1-treated wound. Scale = 1 mm.

ACT: α-connexin carboxyl terminal; CT: Carboxyl terminal; Cx43: Connexin43; ZO: Zonula occludens.

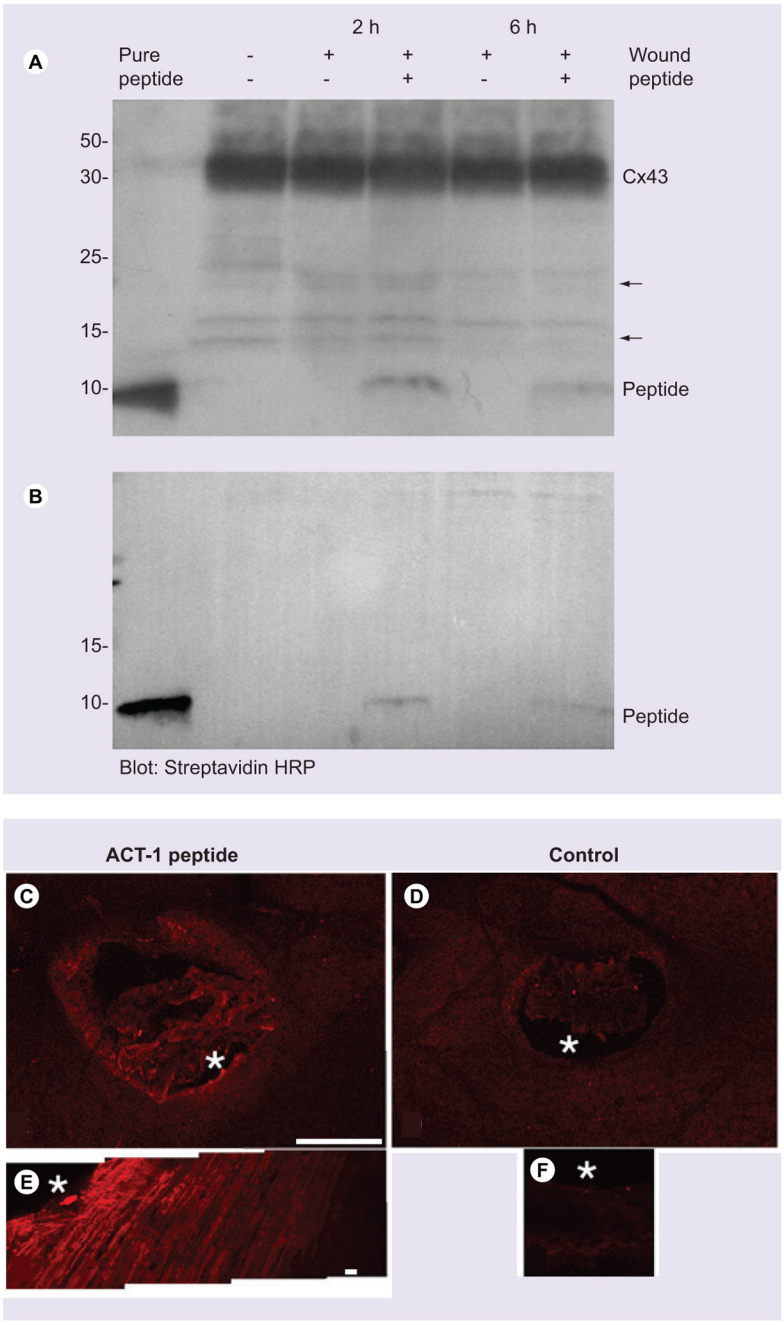

Figure 2. ACT1 turnover and distribution in skin wounds

(A & B) blots detecting ACT1 (< 10 kDa) in unwounded skin (−) or in wounded (+) skin not treated (−) or treated (+) with ACT1 peptide 2 and 6 h postwounding in neonatal mice. In **(A)** peptide is detected using an antibody against the Cx43 CT and **(B)** by streptavidin HRP (GE Healthcare, Piscataway, NJ, USA). Note: pure ACT1 peptide (120 ng peptide) is run in the first lane. **(C)** Shows ACT1 distribution in tissue surrounding a wound on a neonate 2 h following treatment as detected by streptavidin (Alexa 594)-labeling. In **(E)** a montage of confocal optical sections (at a location indicated by the asterix on **(C)**) shows uptake of ACT1 by cells. **(D)** and **(F)** show vehicle control wounds with no detectable fluorescent signal following streptavidin (Alexa 594)-labeling. Scales: **C & D** = 1 mm, **E & F** = 100 μm.

ACT: α-connexin carboxyl terminal; CT: Carboxyl terminal; Cx34: Connexin34; HRP: Horse radish peroxidase.

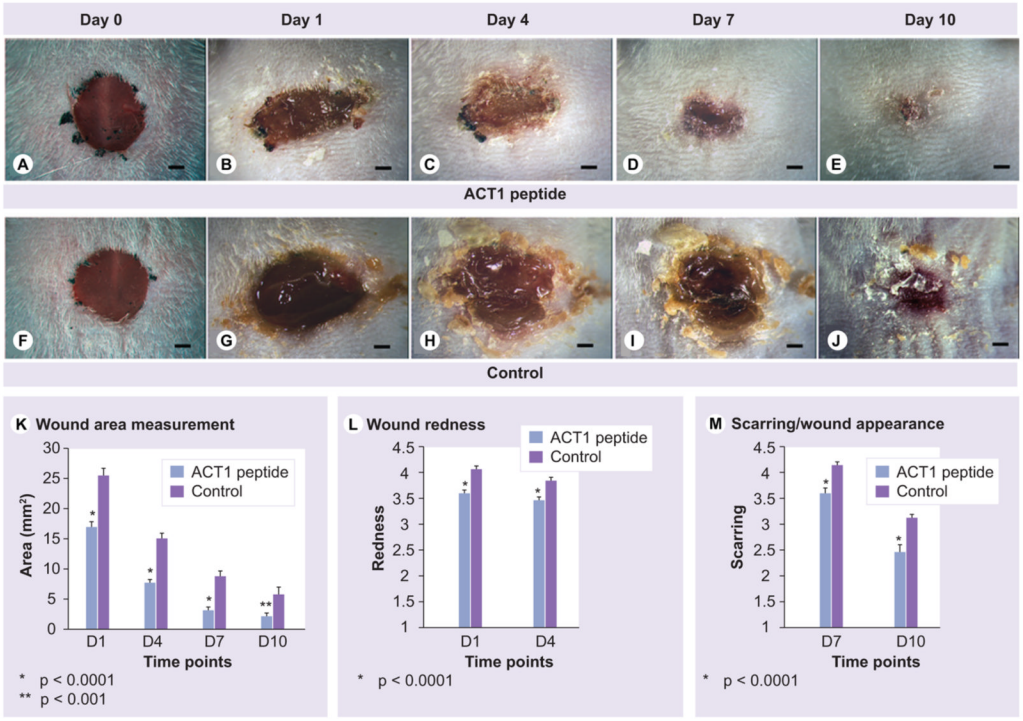

Figure 3. ACT1 affects on skin wound healing on adult mice

Healing of 5 mm excisional wounds on adult mice over 10 days following wounding and ACT1 treatment **(A–E)** versus a vehicle control **(F–J)**. Figure **(K)** is a quantitative demonstration that ACT1-treated wounds (n = 102, blue bars) are significantly smaller in size at 24 h, 4, 7 and 10 days as compared with controls (n = 95, purple bars). Wound redness in the same wounds measured for closure is significantly decreased at 24 h and 4 days postwounding **(L)** and scarring/overall appearance is significantly improved at 7 and 10 days postwounding **(M)** after ACT1 peptide treatment compared with controls. Scale A–J = 1 mm.

ACT: α-connexin carboxyl terminal. that relative to controls, closure was significantly enhanced within 24 h of treatment by ACT1

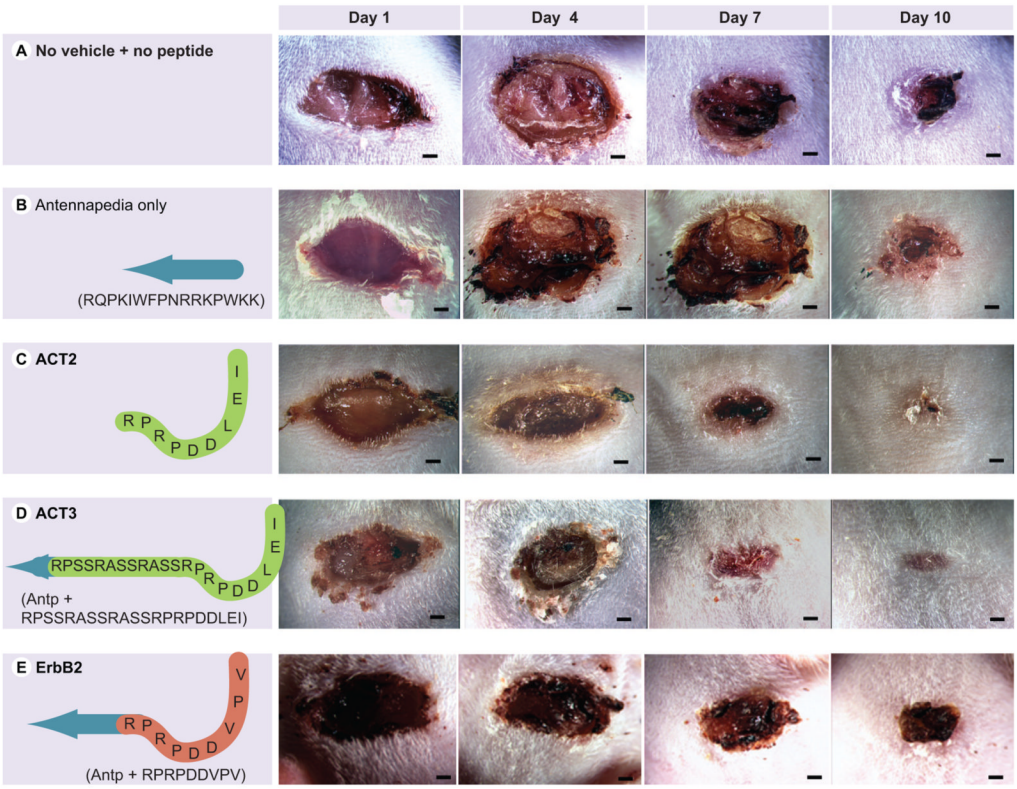

Figure 4. Peptides related to ACT1

Row **(A)** is a single wound representative of seven untreated control wounds that received neither pluronic vehicle nor peptide treatment. The second row **(B)** is representative of nine wounds receiving a peptide corresponding to the 16 amino acid antennapedia sequence (blue arrow) of ACT1. This peptide, and the other three peptides in Figure 4 were delivered in a manner identical to that used for ACT1 treatment; for instance, at 60 μM in 100 μl 20% pluronic gel at time of injury and 24 h later. The third through fifth rows **(C, D & E)** show representative wounds (of 7–10 wounds for each peptide) treated with ACT2 **(C)**, a peptide comprising the CT-most nine amino acids of Cx43 without N-terminal antennapedia, ACT3 **(D)**, including the CT-most 21 amino acids of Cx43, and ErbB2 **(E)**, incorporating the class II PDZ-binding motif of ErbB2. Scale = 1 mm.

ACT: α-connexin carboxyl terminal; Antp: Antennapedia; CT: Carboxyl terminal; Cx43: Connexin43; PDZ: Postsynpatic density 95/discs large/zonula occludens-1.

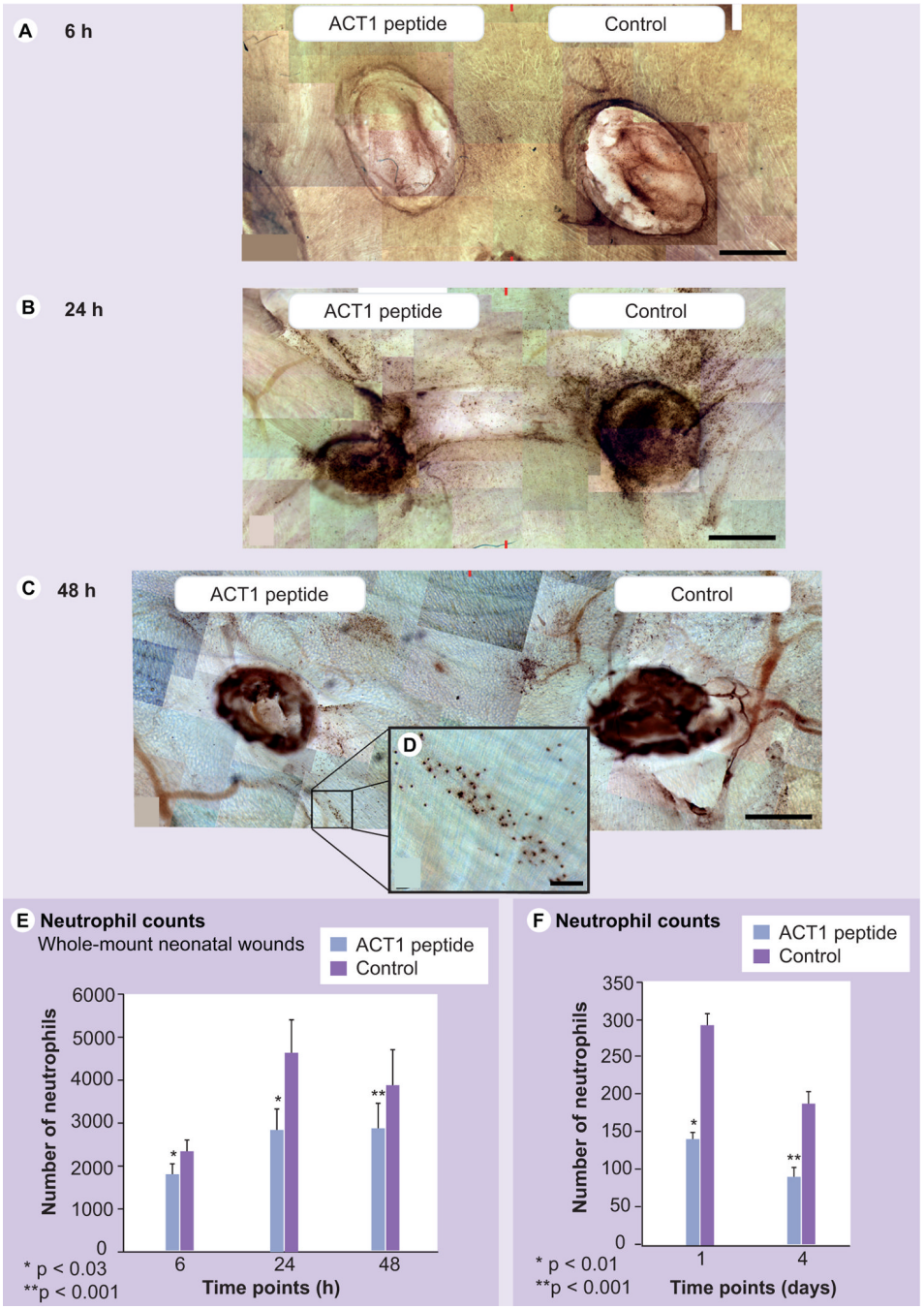

Figure 5. ACT1 affects on initial inflammatory response following skin wounding

The effect of ACT1 on neutrophil density in control/treatment pairs of excisional wounds from neonatal mice at **(A)** 6 h (n = 6), **(B)** 24 h (n = 7) and **(C)** 48 h (n = 8) postwounding. Photomontages of the underside of whole-mount myeloperoxidase-stained skin samples are shown following fixation and benzobenzoate clearing to transparency. Red marks at the top and bottom of each montage indicate the midline edge of control and ACT1 measurement fields. The density of neutrophils at ACT1-treated wounds (left) is lower at all time points than at control wounds (right) on the same animal, most notably at 24 h. Inset on **(C)** shows higher magnification of individually labeled neutrophils associated with a vessel-like structure adjacent to an ACT1-treated wound 48 h postwounding **(D). (E)** There are significant

reductions in density of neutrophils at ACT1-treated wounds relative to paired control wounds at each time point. **(F)** Neutrophils were also significantly reduced in ACT1-treated (blue bars) and control (purple bars) wounds at 1 and 4 days postinjury. Scale: A–C = 250 μm, Inset = 50 μm.

ACT: α-connexin carboxyl terminal.

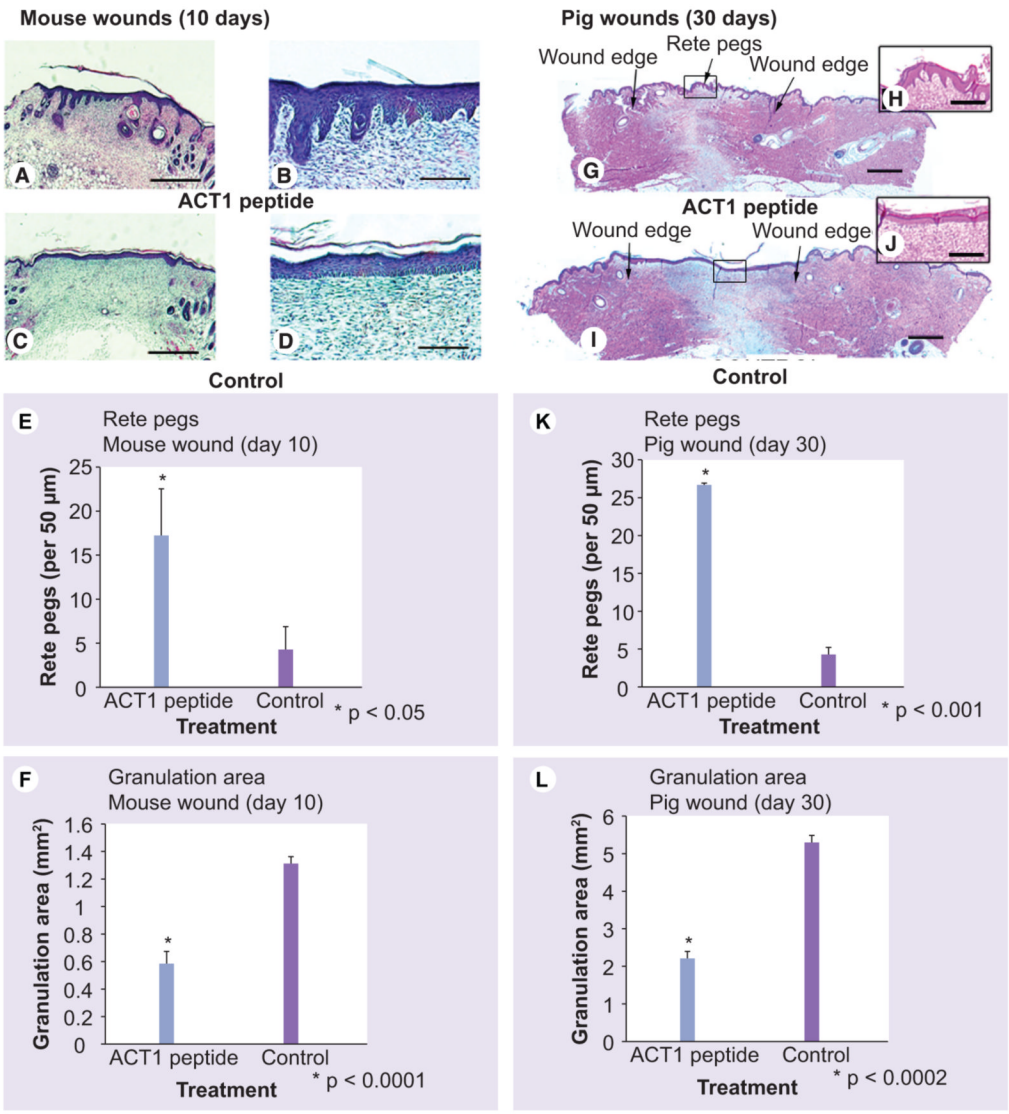

Figure 6. ACT1 affects on area of granulation tissue and rete peg density

(A–D) H&E histology of healed excisional wounds on adult mice 10 days postwounding following treatment with ACT1 **(A & B)** or vehicle control **(C & D). (B & D)** provide higher magnification details from **(A & C)**, respectively. Quantification of rete peg number **(E)** and granulation tissue **(F)** in the healed mouse wounds (ACT1 n = 4, blue bars, control n = 4 purple bars). **(G–J)** H&E histology of healed excisional wounds in pig 30 days postwounding following treatment with ACT1 **(G & H)** (n = 3) or vehicle control **(I & J)** (n = 3). The insets in **(H & J)** provide details from **(G & I)**, respectively. Rete peg numbers **(K)** and granulation tissue amounts **(L)** in pig wounds. Scale: **(A & C)** = 0.5 mm, **(B & D)** = 2 mm, **(G & I)** = 1mm and **(H & J)** = 125 µm.

ACT: α-connexin carboxyl terminal.

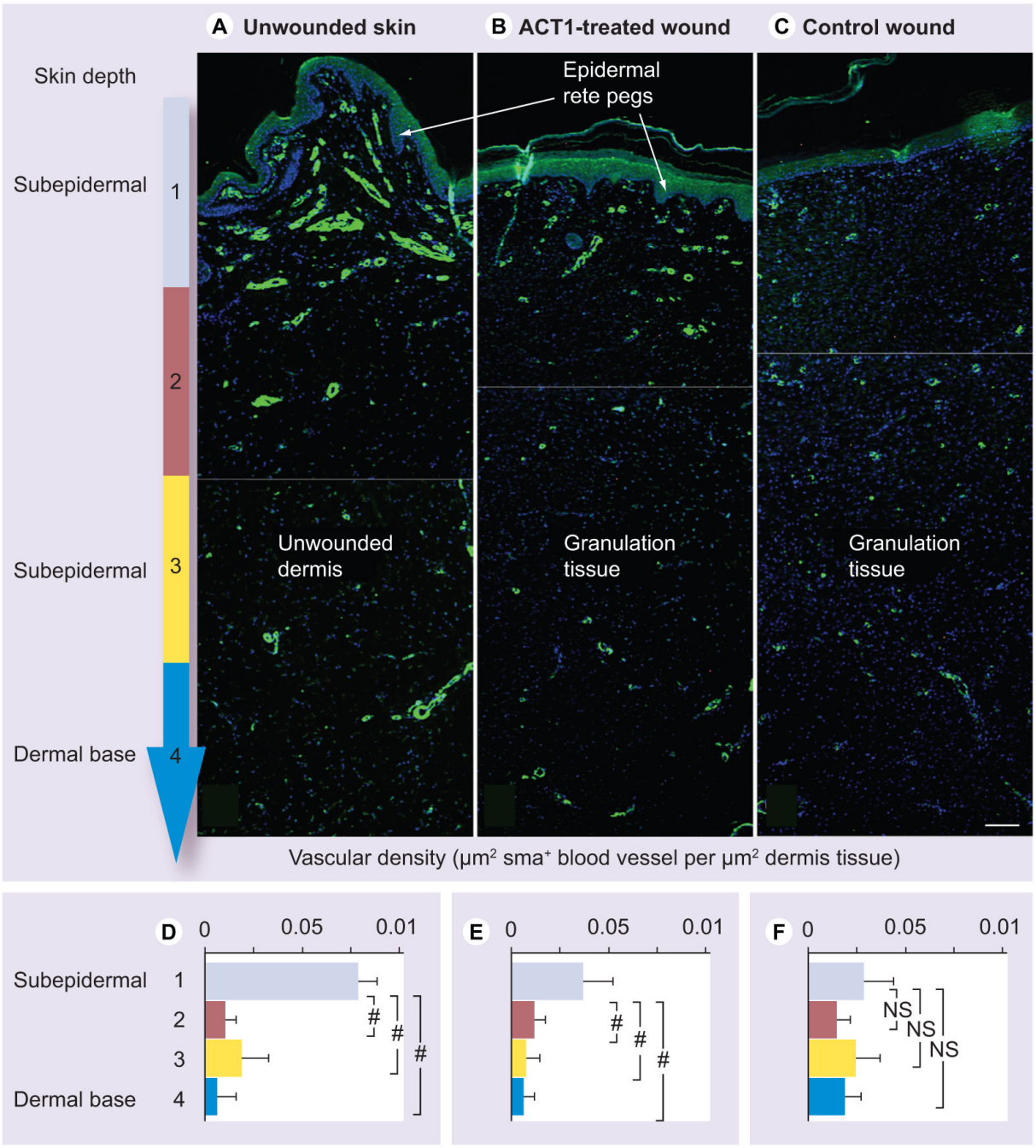

Figure 7. ACT1 affects on granulation tissue vascularization pattern in pig wounds

(A–C) Montages of histological sections through pig skin immunolabeled for sma. The sections are normal to the skin surface and span the epidermis (top) to the base of the dermis. Green fluorescent signal discloses sma^+ blood vessels. The light blue, red, yellow and dark blue colored bars to the left of **(A)** divide the dermis into approximate quartile regions of depth. **(B&C)** are through healed (30 days postinjury) ACT1-treated and vehicle control wounds (sister sections to 6G and 6I respectively). Scale = 1 mm. **(D–E)** Quantification of sma -labeling in **(D)** unwounded skin, **(E)** ACT1-treated and **(F)** vehicle control wounds confirm that only the superficial dermal quartile (light blue) of unwounded and ACT1-treated skin is significantly

higher than deeper quartiles 2 (red), 3 (yellow) and 4 (dark blue). No significant variation in vascular density is seen in the control granulation tissue.
ACT: α-connexin carboxyl terminal; NS: Not significant; sma: α-smooth muscle actin.

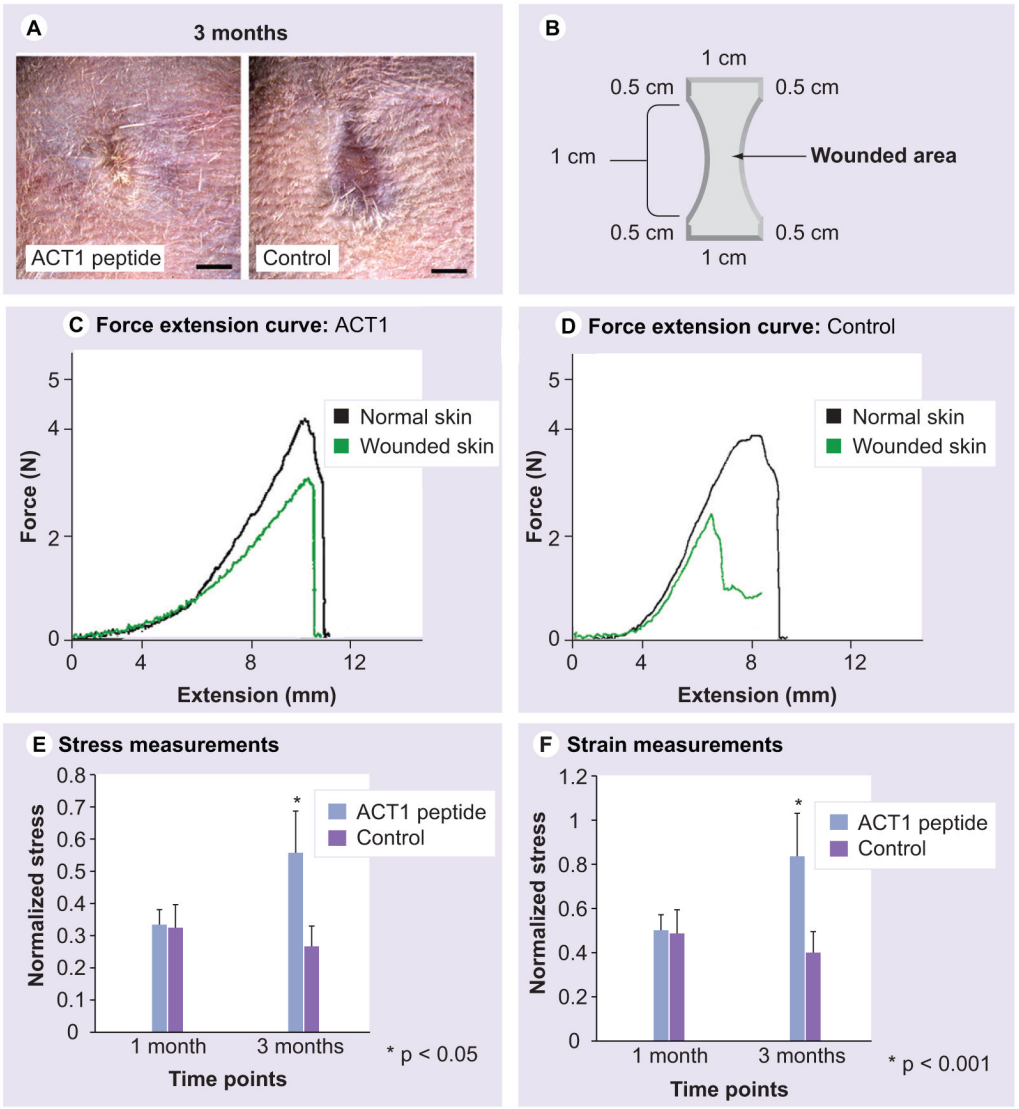

Figure 8. ACT1 affects on mechanical properties of healed skin wounds in mice

(A) Representative images of 3-month-old healed wounds used for mechanical testing. Scale bar = 1 mm. **(B)** A representative force–extension curve of a skin strip from a healed wound (green) superimposed on a curve from an adjacent strip of unwounded skin (black) from the same animal. **(C & D)** Representative force–extension curves from ACT1 -treated and control-healed wounds (green) superimposed on curves from adjacent unwounded skin (black) from the same animal. Healed wounds treated with ACT1-peptide (blue bars) or vehicle control solutions (purple bars) were assessed for stress **(E)** and strain **(F)** at failure of the skin strip at 1 and 3 months postwounding.

ACT: α-connexin carboxyl terminal.

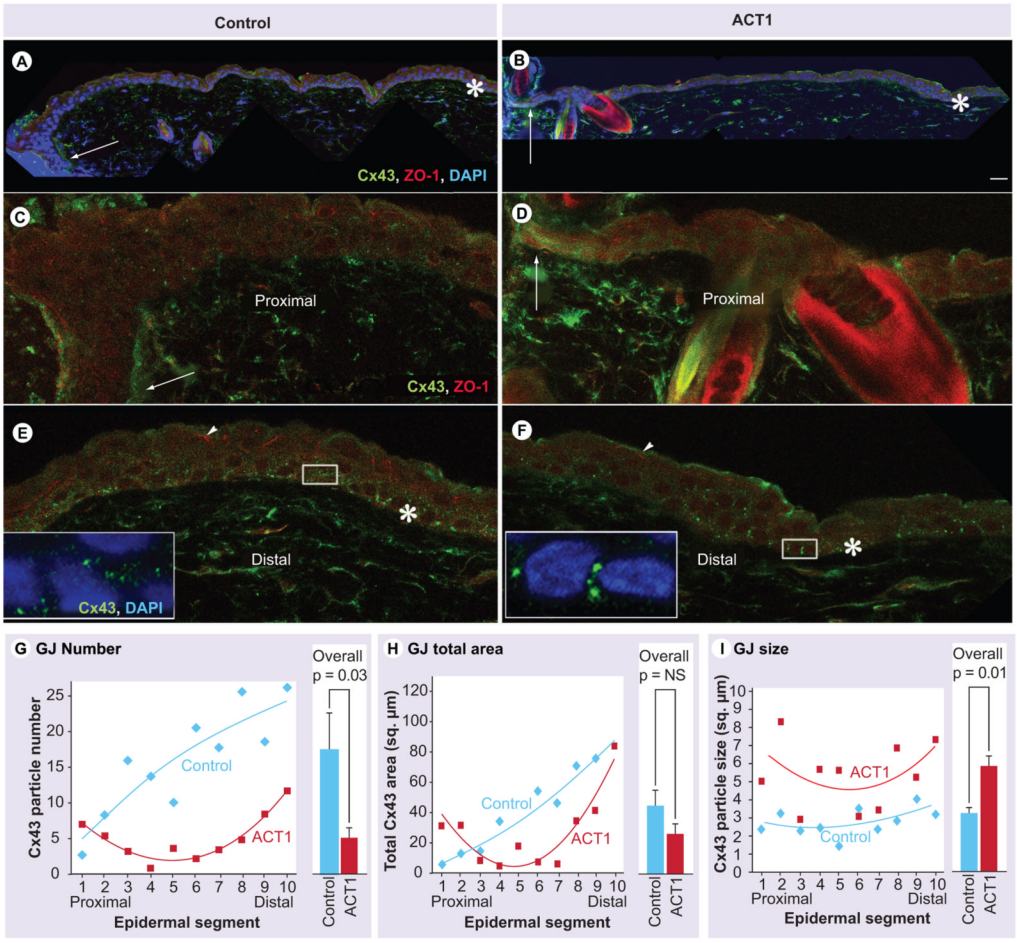

Figure 9. ACT1 affects on Cx43 organization in mouse wound epidermis

(A & B) Montages of confocal images of control **(A)** and ACT1-treated **(B)** wound edges 24 h after injury. Scale bar **(B)** = 20 µm. The sections have been triple labeled using Cx43 (green) and ZO-1 (red) antibodies and the nuclear label DAPI (blue). Large arrows indicate epidermal cells proximal to the wound edge. Asterisk indicates distal epidermal cells, 80–120 basal cells back from the wound edge. **(C, D, E & F)** provide high-magnification confocal images of Cx43 and ZO-1 immunolabeling in the proximal and distal epidermal regions of the montages shown in A and B. Large arrows and asterisks in **(C, D, E & F)** correspond to the locations indicated in **(A & B)**. Note that blue nuclear signal is not shown. The small arrowheads in **(E & F)** are stripe-like accumulations of ZO-1 labeling between apical epidermal cells. The large bright red/yellow objects in **(F)** are hair follicles. Insets in **(E & F)** are higher-magnification views of the boxed regions. **(G, H & I)** are plots of quantitative data from paired control and ACT1-treated wounds on five mice. Shown are segment to segment variation along the wound epidermis in Cx43 particle (i.e., GJ aggregates) number **(G)**, total area of Cx43 GJ immunolabeling **(H)** and Cx43 particle size from the segment most proximal to the wound edge (epidermal segment 1) to the most distal (epidermal segment 10). Each segment contains ten basal keratocytes in sequence. Regression lines represent a two-factor polynomial best fit to the variance patterns along the epidermis. Bar graphs of the overall mean and standard error pooled from the ten segments is given alongside the scatter plots for particle number and size, and total Cx43 area.

ACT: α-connexin carboxyl terminal; Cx43: Connexin43; GJ: Gap junction; NS: Not significant ($p > 0.05$); ZO: Zonula occludens.